Deep-Sea Research Part I 124 (2017) 140–152

Contents lists available at ScienceDirect

Deep-Sea Research Part I

journal homepage: www.elsevier.com/locate/dsri

Observing the subsurface thermal signature of the Black Sea cold intermediate layer with Argo profiling floats

Anil Akpinar*, Bettina A. Fach, Temel Oguz

Institute of Marine Sciences, Middle East Technical University, Erdemli, Turkey

ARTICLE INFO

Keywords:
Black Sea
Argo floats
Cold intermediate layer
Water mass formation
Climatic variations

ABSTRACT

Cold intermediate layers (CILs) constitute a key indicator of the subsurface thermal signature in many marginal and subarctic seas. Towards better understanding the impacts of natural and anthropogenic climate variability in the Black Sea, the present study elucidates processes leading to the observed changes of CIL characteristics at mesoscale and monthly-to-interannual scales by analyzing weekly temperature-salinity profiles provided by Argo floats for 2002–2015. The continuous time series data allowed to elucidate different types of CIL formation episodes. For the first time, it was possible to trace their subsequent evolution depending on the number and intensity of successive, but often intermittent, autumn-winter cooling events in addition to the ambient flow and stratification characteristics within the cyclonic interior and anticyclonic coastal eddies/gyres. The spatial distribution of CIL formation in the cold years 2003, 2006 and 2012 covered much of the Black Sea, even coastal anticyclonic eddies as a new feature which has not been documented before. The data also recorded modification of CIL during the rest of the year in terms of its thickness, position, temperature and salinity ranges in response to advective transport by the circulation system, interior turbulent mixing, and quasi-lateral intrusions associated with mesoscale features.

1. Introduction

Cold intermediate layers (CILs) are common thermal features observed in many coastal, marginal, and subarctic seas. They form as a result of intense cooling of surface waters during winter and prevail in the form of distinct subsurface water mass during the rest of the year when the surface mixed layer is stratified by warming, sea-ice melt, or increased river runoff. CILs may vary regionally in terms of their vertical coverage, heat content, and water mass characteristics at their formation sites. In the Black Sea, the CIL structure is conventionally identified by temperatures less than 8 °C and its vertical extent is limited to the upper 100 m layer, corresponding typically to ~15.4 kg m^{-3} isopycnal. The Black Sea cold intermediate water formation is, therefore, a shallow, depth-limited version of an order of magnitude deeper dense-water mass formation process observed in weakly stratified systems such as those observed in the Rhodes basin of the Eastern Mediterranean (The Liwex Group, 2003) and the Liguro-Provencal basin of the Western Mediterranean (MEDOC Group, 1970; Smith et al., 2008). The Black Sea is characterized by a strong and permanent two-layer stratification that separates well-mixed surface waters from anoxic deep water (Ozsoy and Unluata, 1997). The permanent pycnocline is preserved due to saline waters entering from Bosphorus Strait and freshwater input from rivers. During winter, a relatively cold but less saline water mass is formed in the northwestern shelf region (Mihailov et al., 2016) in contrast to slightly warmer but more saline CIL waters forming over isopycnal domes of the interior basin (Oguz and Besiktepe, 1999; Gregg and Yakushev, 2005; Korotaev et al., 2014; Capet et al., 2014). Strong density stratification of $2.0-2.5$ kg m^{-3} across the permanent pycnocline (75–150 m) limits vertical penetration of the convective mixing and thus confines cold water to the uppermost 50–80 m layer (Oguz, 2002). Following the formation event, cold water is well preserved between the seasonal thermocline and the permanent pycnocline (Ovchinnikov and Popov, 1987; Murray et al., 1991; Oguz et al., 1993, 1994; Ozsoy and Unluata, 1997; Stanev et al., 2003; Belokopytov, 2011; Krivosheya et al., 2012; Alkan et al., 2013) because of extremely low vertical diffusion rates on the order of 10–6 m^2 s^{-1} below the surface mixed layer (Gregg and Yakushev, 2005; Zatsepin et al., 2007).

The CIL formation process is initiated by the preconditioning phase, in which progressive cooling in late-autumn leads to a more organized cyclonic rim current circulation and a more pronounced “doming” of the isopycnal surfaces within the interior region. This process causes upwelling of relatively dense deep waters and further intensifies the permanent pycnocline but weakens the static stability of the surface

* Corresponding author.
E-mail address: anil@ims.metu.edu.tr (A. Akpinar).

http://dx.doi.org/10.1016/j.dsr.2017.04.002
Received 13 June 2016; Received in revised form 27 March 2017; Accepted 1 April 2017
Available online 13 April 2017

layer above the pycnocline (Gregg and Yakushev, 2005; Capet et al., 2012). The preconditioning phase is followed by the cold water formation phase in January/February in response to increased latent heat loss by successive episodes of very cold air temperatures. The density increase associated with these cooling events is, however, not sufficiently strong to break down the high stratification at the permanent pycnocline. The convective mixing phase over the domes of interior cyclonic gyres is followed by an isopycnal spreading phase of the newly formed cold water mass toward the periphery of the basin (Oguz and Besiktepe, 1999).

Our current knowledge on the formation and spreading of CIL is limited to scattered and unsystematic measurements. In this study, we make use of more than a decade-long (2002–2015) temperature and salinity measurements of weekly profiling Argo floats for a thorough examination of the Black Sea surface and cold intermediate water mass characteristics at subinertial (weekly-monthly) to interannual scales. This is the first time that the water mass properties of the upper layer water column are resolved by the weekly temperature, salinity profiles over a decade with the spatial coverage of the entire deep basin of the Black Sea. The main objective is thus to improve our limited knowledge on the spatial and temporal variability of cold intermediate water formation under different hydro-meteorological conditions, and subsequent distribution and transformation characteristics in relation to the large and mesoscale circulation features and interior mixing processes. The present study complements earlier studies based on the analyses of Black Sea Argo float data devoted to the intensity and variability of intermediate and deep currents (Korotaev et al., 2006) and the subsurface oxygen structure and the ventilation of subsurface water masses near the oxic-anoxic interface (Stanev et al., 2013; Capet et al., 2016).

2. Observations and methods

Seven profiling floats were deployed in the Black Sea between 2002 and 2006 within central parts of the western basin (Table 1). This initiative was a result of the collaboration between the Office of Naval Research, School of Oceanography-University of Washington (USA), Institute of Marine Sciences-Middle East Technical University (Turkey), and the Marine Hydrophysical Institute-Ukrainian Academy of Sciences. The floats operated between 2002 and 2009. Additional float data were collected during 2009–2015 within the framework of Euro-Argo program (http://www.euro-argo.eu/), the European contribution to the global Argo initiative (Argo, 2000) that are available for download at http://www.coriolis.eu.org. Operational periods, the parking and profiling depths, and code numbers of the floats used in this study are listed in Table 1. Floats provided vertical profiles of temperature, salinity, and density from surface to the depth of 500–1550 m at 1 m bins once a week and continued drifting at their respective parking depths. The accuracy of Argo temperature, salinity, and pressure sensors are generally better than 0.005 °C, 0.01, and 5 m respectively (ARGO Science Team, 2000; Korotaev et al., 2006). Quality of the Argo data was checked using the quality flags of the data itself, followed by a test for impossible location, pressure, temperature and salinity values, as well as a careful inspection of suspicious profiles following T/S diagrams and comparison with neighboring profiles. Some occasional gaps exist in the data set due to omission of some data not passing the quality checks. This particularly applies for the salinity

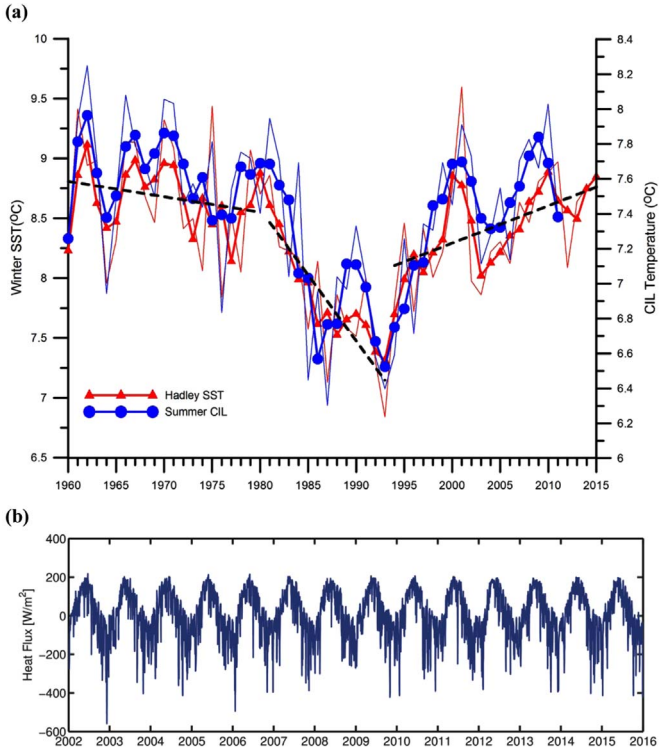

Fig. 1. a) Long term variations of the winter (December-March) mean sea surface temperature calculated from Hadley Data (red lines and symbols) and the summer-autumn (May-November) mean CIL temperature from Belokopytov (2011) (blue lines and symbol). The thin lines with symbols refer to the original data whereas the thick curves represent their variations smoothed by three-point moving averages. The dashed lines represent two successive cooling trends (1960–1980 and 1980–1993) and a subsequent warming trend (1993–2013) calculated from the Hadley SST data. (b) Variations of basin-wide, daily surface heat flux (W m^{-2}) calculated from ERA-Interim data for 2002–2015. (For interpretation of the references to color in this figure legend, the reader is referred to the web version of this article.)

Table 1
Parking depth, profiling depth and operation time frame of the floats used in this study.

Float no	Deployment location	Parking Pressure (dbar)	Profiling Pressure (dbar)	Start date: (dd/mm/yyyy)	End date: (dd/mm/yyyy)	Duration (~months)
BS0587	42.25°N, 30.34°E	1550	1550	02.09.2002	21.02.2004	18
BS0631	41.83°N, 29.83°E	750	1550	02.09.2002	21.12.2004	28
BS0634	42.24°N, 30.33°E	200	1550	02.09.2002	16.04.2005	32
BS1325	41.88°N, 29.59°E	500	1550	07.03.2005	18.01.2009	47
BS1550	41.87°N, 29.56°E	1000	1550	07.03.2005	02.10.2008	43
BS2206	42.14°N, 30.26°E	1550	1550	12.06.2006	22.02.2009	33
BS2619	42.15°N, 30.26°E	1550	1550	12.06.2006	23.12.2009	43
6900805	42.95°N, 28.946°E	750	1500	19.03.2011	15.08.2015	–
1901200	42.88°N, 28.83°E	200	1550	08.12.2009	22.02.2013	39
6901961	43.17°N, 30.76°E	200	1500	06.11.2012	15.08.2015	35
6901896	41.78°N, 32.89°E	200	750	04.08.2013	05.10.2014	14
7900466	43.98°N, 31.99°E	450	500	06.06.2009	27.12.2012	43

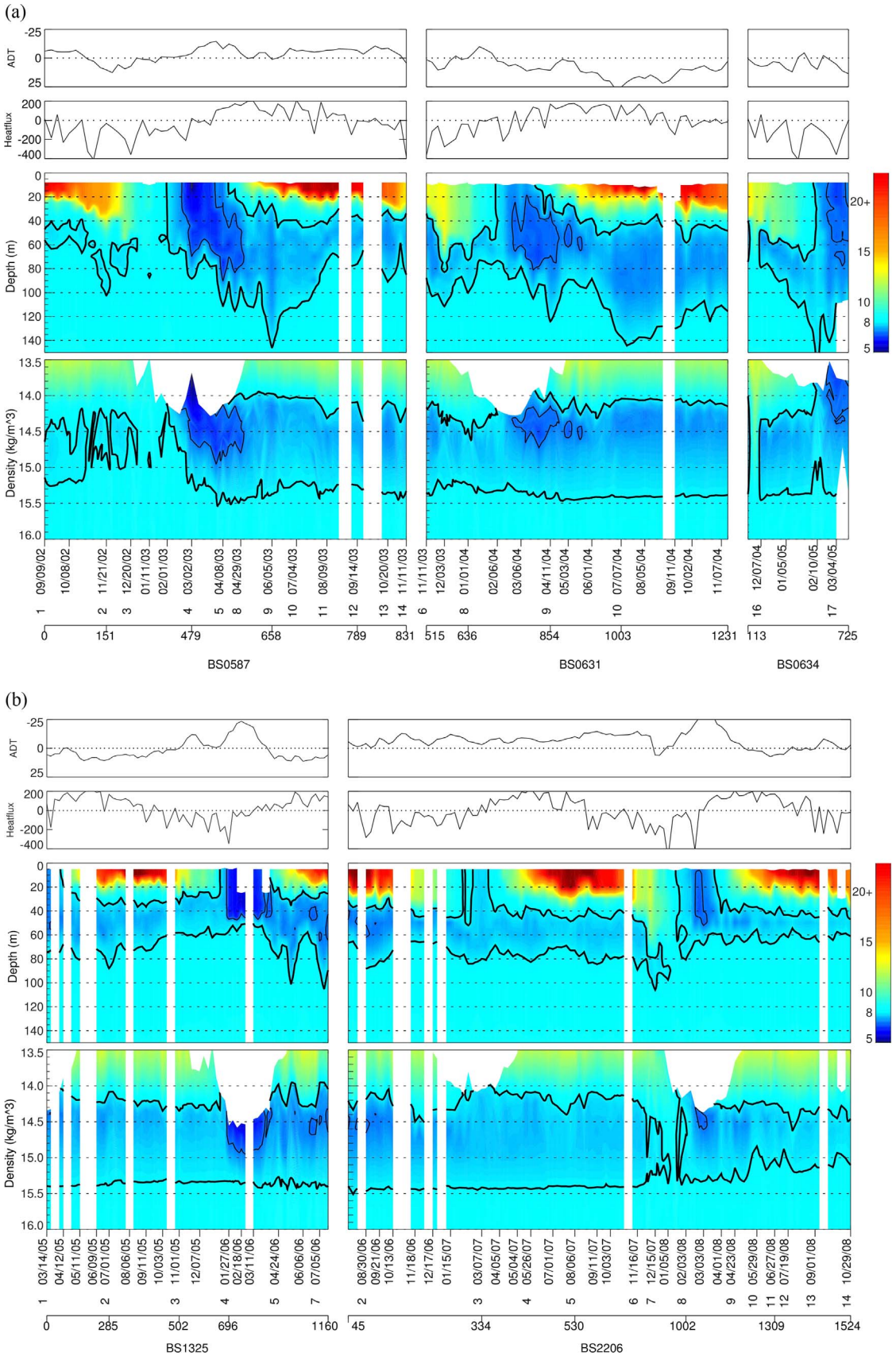

Fig. 2. Contour plots of temporal temperature variation vs depth within the upper 150 m layer plotted above contour plots of temperature variation vs density (kg m^{-3}) constructed using different Argo float trajectories (a) along the southern rim current zone during 2002–2005, (b) within the west-central interior basin during 2005–2009, (c) within the southeast basin during 2005–2009. Thick black contour lines mark the 8 °C isotherm which encloses the CIL with colder temperatures, thin black line marks the 7 °C isotherm. White vertical stripes indicate missing data. Dates are given along the x-axis in the form of month/day/year, and the numbers located below the dates refer to float locations as shown in Fig. 3. Float numbers are indicated along the x-axis. The second x-axis represents the distance traveled in km. Above the contour plot absolute dynamic topography (cm) and total heat flux (W/m^2) data along the float trajectory is displayed.

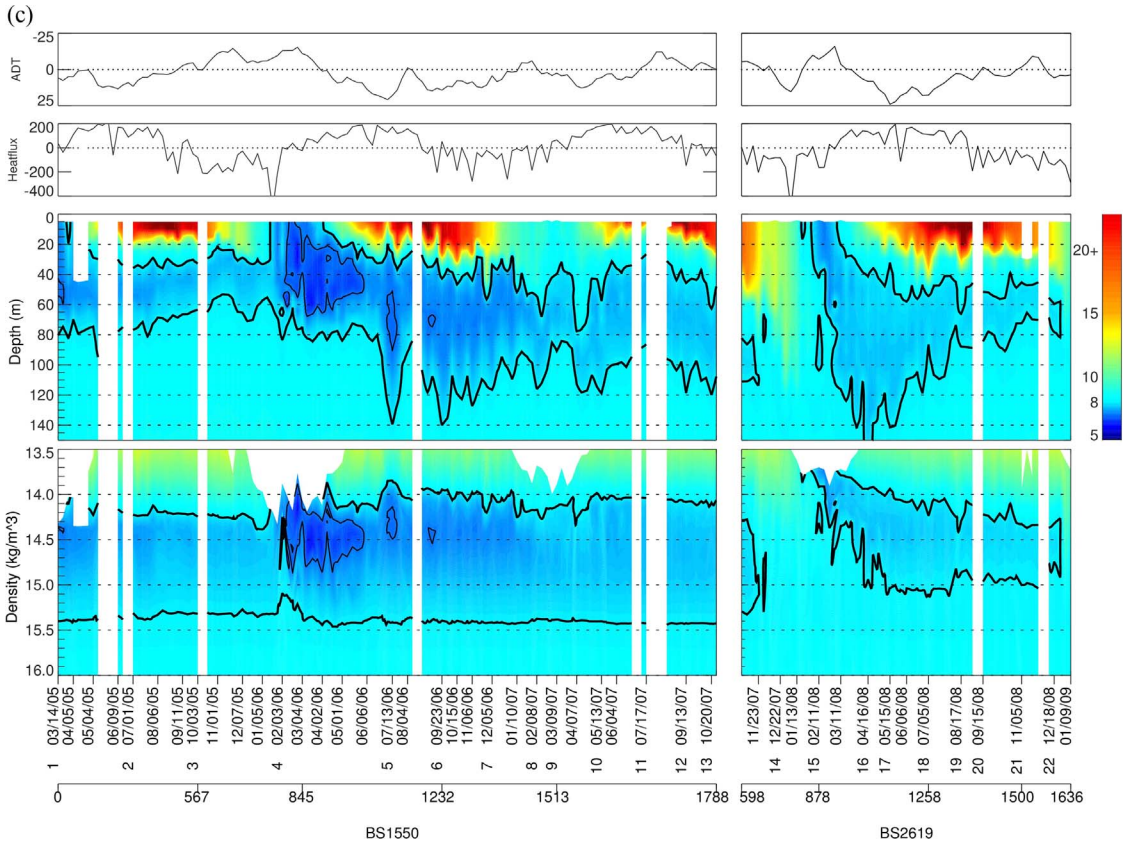

Fig. 2. (*continued*)

profiles of floats deployed after 2011.

In this study the Argo float data were complemented by sea surface temperature, summer-autumn (May-November) mean CIL temperature, sea surface height anomalies, as well as model derived heat flux data. The monthly mean SST data set was provided by Hadley Centre, UK Met Office (http://www.metoffice.gov.uk/hadobs/hadisst/) (Rayner et al., 2003). Here it was averaged over the winter months (December-March). Similarly, the monthly mean CIL data from 1960 to 2011 were provided by Belokopytov (2011) for the interior part of the basin with water depths greater than 200 m. The monthly data represent averages of temperatures less than 8 °C (Belokopytov, 2011) but they are further averaged over summer-autumn (May-November) of each year.

For further interpretation of Argo data in terms of prevailing circulation features along trajectories the weekly, delayed-time, merged sea surface height anomalies distributed by AVISO (Archiving, Validation and Interpretation of Satellite Oceanographic Data) (http://www.aviso.oceanobs.com/las/) were used. Absolute dynamic topography (ADT) was calculated from this data by adding the mean dynamic topography calculated by Korotaev et al. (2003) to the weekly sea surface height anomalies. In addition, the ERA-interim surface heat flux data set (http://data-portal.ecmwf.int) was used to estimate the degree of winter cooling. Both, the absolute dynamic topography and heat flux data were interpolated onto the $0.1 \times 0.0625^{\circ}$ spatial grid, and the absolute dynamic topography data were interpolated in time to daily fields using an optimal interpolation technique. Then, both heat flux and sea surface height were extracted along Argo float trajectories are used to estimate heating/cooling processes affecting CIL formation and the position of the floats in cyclonic or anticyclonic regions.

3. Results

3.1. Long-term changes in the CIL temperature

In order to put the results of the Argo profiling float data into the context of long-term climate-induced changes, we first look at inter-annual variations of the mean winter (December-March) sea surface temperature (SST) and the mean summer-autumn (May-November) CIL temperature since 1960 (Fig. 1). Both followed decadal-scale oscillations in the form of two successive cooling phases (1960–1980 and 1980–1993) and a subsequent warming phase (1993–2013) as shown by the linear regression lines (Fig. 1). Earlier studies showed that the North Atlantic Oscillation (NAO) (Oguz et al., 2006; Oguz, 2011) was the primary mechanism to induce these decadal-scale cooling and warming phases. Capet et al. (2012) showed that the shorter (1–5 years) oscillations are driven by the East-Atlantic West-Russia (EA-WR) oscillation and thus most of the climate-induced variability in the Black Sea was regulated by the combined impact of these patterns (Kutiel and Benaroch, 2002; Oguz et al., 2006; Capet et al., 2012). The synchronous variations of mean winter surface temperature and mean summer-autumn CIL temperature were expected because the winter cold water mass structure (as shown by the SST) was transformed later into subsurface cold water mass structure following the development of the seasonal thermocline. 1981–1985 and 1993–1998 were two anomalous periods of rapid cooling and warming, respectively. 1987 and 1993 were particularly cold years characterized by nearly a 1 °C temperature reduction with respect to the previous year. A similar level of the temperature reduction was also encountered during February-March 2003, 2006, and 2012 (see also Fig. 9a). On the other hand, the CIL structure was almost lost during warm years 2001 and 2010–2011 as well as 2014–2015.

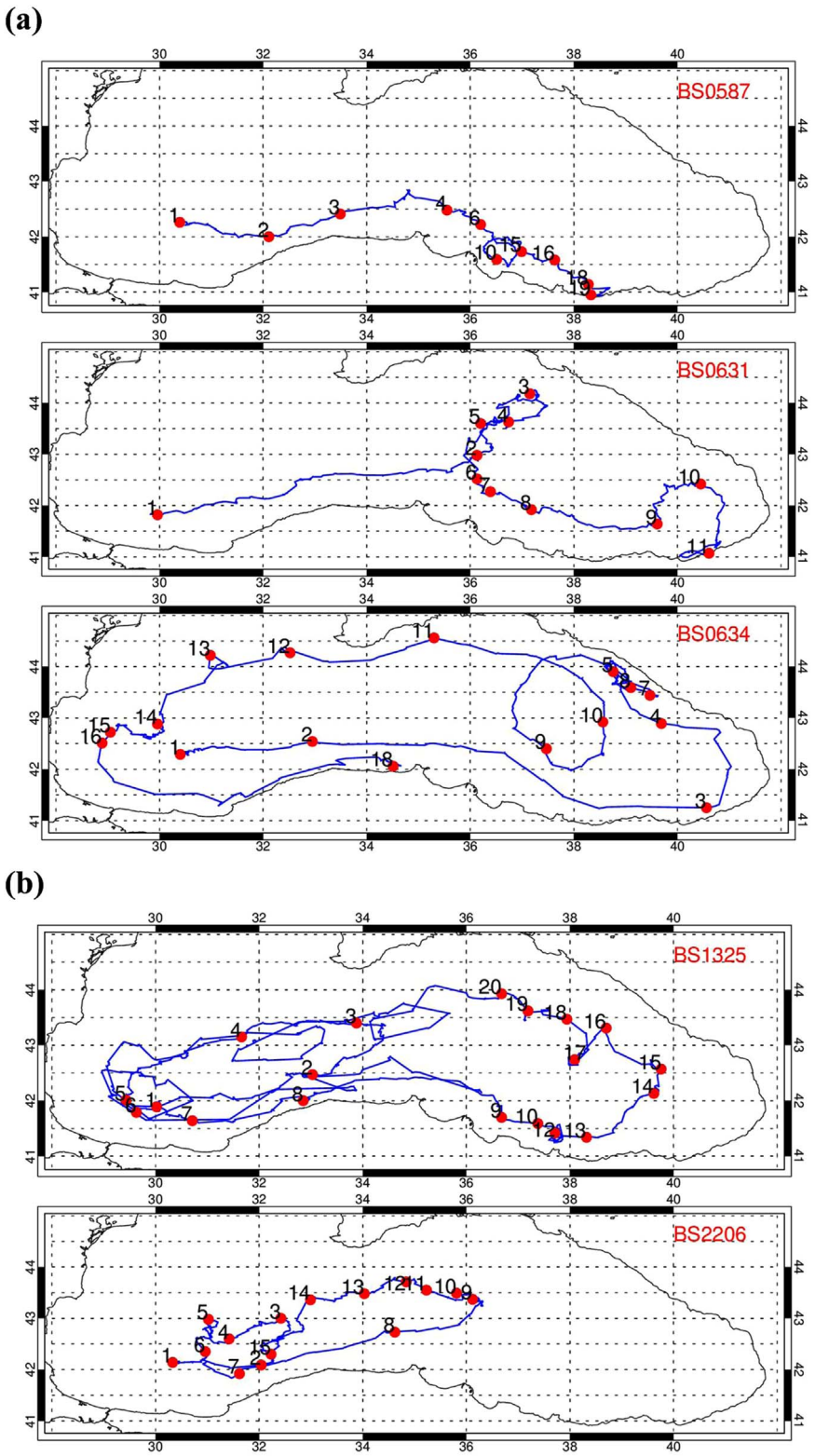

Fig. 3. Argo float trajectories of different floats (a) float BS0587, BS0631, BS0634 used in Fig. 2a, (b) BS1325, BS2206 used in Fig. 2b, and (c) BS1550, BS2619 used in Fig. 2c. Numbers correspond to the locations of the float marked by dates shown in the temperature transects of Fig. 2.

3.2. Regional and temporal cold water mass formation and spreading character

Strong interannual temperature variations within the upper 150 m layer (Fig. 2a–c) characterize different types of cold intermediate water mass formation. Fig. 2a shows these variations for the time frame 2002–2005 using the data compiled from three floats along the southern rim current zone (see float trajectories BS0587, BS0631 and BS0634 in Fig. 3a). The choice of compiling the trajectories of three floats was made to visualize formation events in different locations (BS0634 in the west, BS0587 in the central and BS0631 in the east) along the southern rim current zone during the time frame 2002–2005. Winter 2002 was

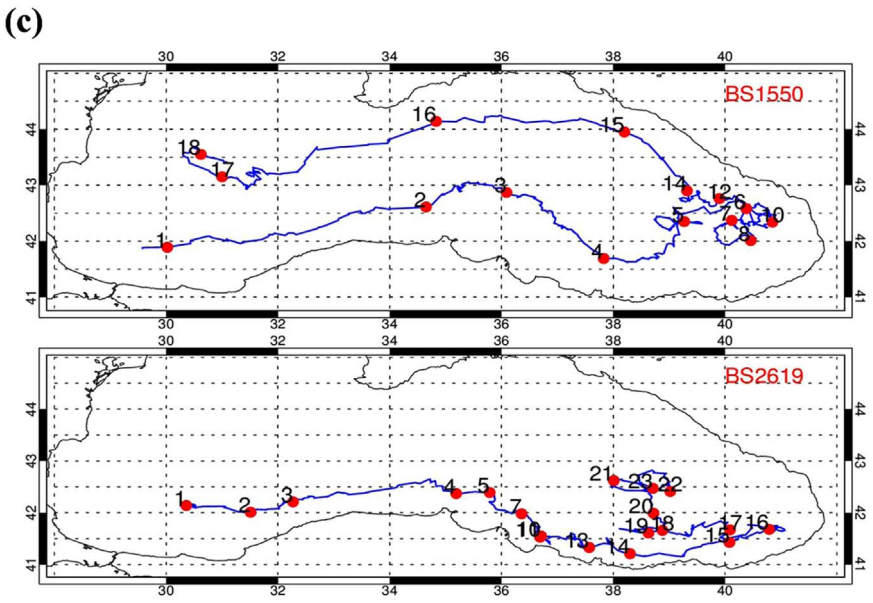

Fig. 3. (*continued*)

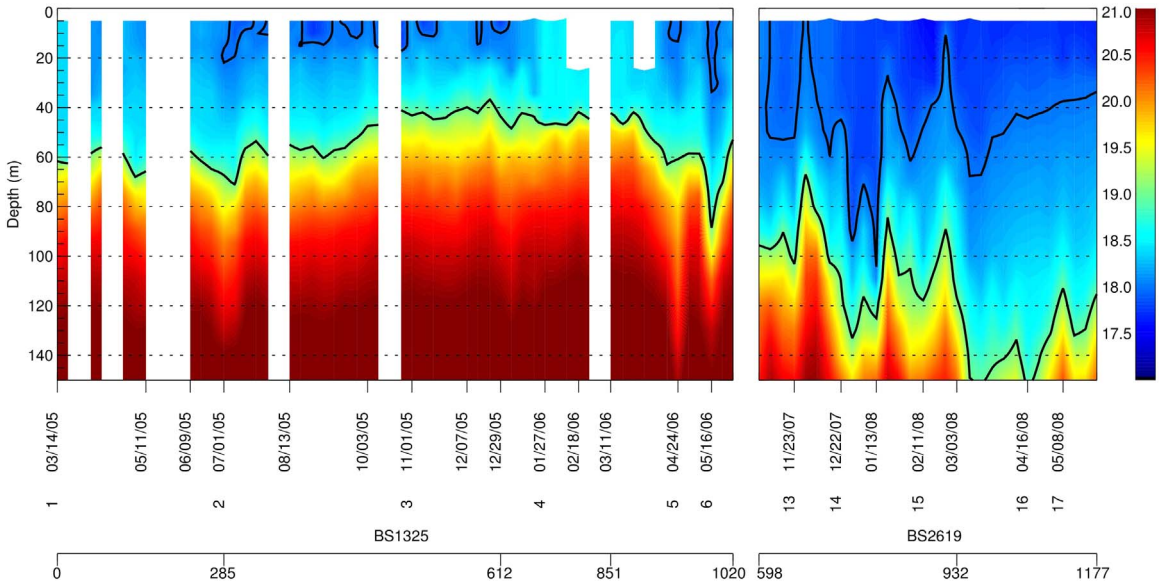

Fig. 4. Contour plots of temporal salinity variations within the upper 150 m layer along the float trajectories within the west-central basin during 2005–2006 (float BS1325) and along the southern coast of the eastern basin during 2007–2008(float BS2619). Thick black contours represent the 18.0 and 19.0 isohalines. White vertical stripes indicate missing data. Dates are given along the x-axis in the form of month/day/year, and the numbers located below the dates refer to float locations as shown in Fig. 3b and c. Float numbers are indicated along the x-axis. The second x-axis represents the distance traveled in km.

relatively mild as reflected by a weak CIL signature whereas winter 2003 was anomalously cold under successive strong cold, dry wind episodes blowing from the northern sector of the Euro-Asia starting by fall 2002. This particularly cold winter was associated with strong positive modes of NAO (Polonsky et al., 2007; Valchev et al., 2012) and EA-WR (Kazmin et al., 2010) leading to an average air temperature of −0.6 °C and sea-water temperature of 5.6 °C on the Romanian shelf (Mihailov et al., 2016). These storm events led to a strong total heat loss up to 400 W m^{-2} as noted along float trajectories in Fig. 2 and by the average value over the basin in Fig. 1b. These episodes led to a progressive reduction of static stability starting as early as November 2002, eroded the CIL by the end of 2002, and generated a rather deep mixed layer covering the entire upper layer with temperatures around 8.5 °C during January 2003 (Fig. 2a). As captured by the float BS0587 within the south-central basin (at location 4 in Fig. 3a), the subsequent cooling episodes continued to cool the uppermost 70–80 m down to 6.0 °C (around 5 °C near the surface) during early March. This event was also captured simultaneously at a nearby location by float BS0631 (location 2 in Fig. 3a), and at a coastal site of the southeastern basin (location 3 in Fig. 3a) by float BS0634, however, they are not shown in Fig. 2a.

Stratification was established by the onset of spring warming in April 2003, and a shallow warm surface mixed layer capped the newly formed cold water starting in May 2003. In the meantime, the float BS0587 drifted to the east and converged into a coastal anticyclonic eddy (at location 9/10 in Fig. 3a) where the CIL lower boundary (represented by the 8 °C isotherm) deepened to nearly 120 m and the CIL core temperature increased by about 1 °C due to vertical mixing and advective processes. When the float left the coastal anticyclone later, the CIL attained again its more typical deep basin structure between 40 m and 80 m depths during rest of 2003.

Cold water mass formation and spreading episodes were repeated

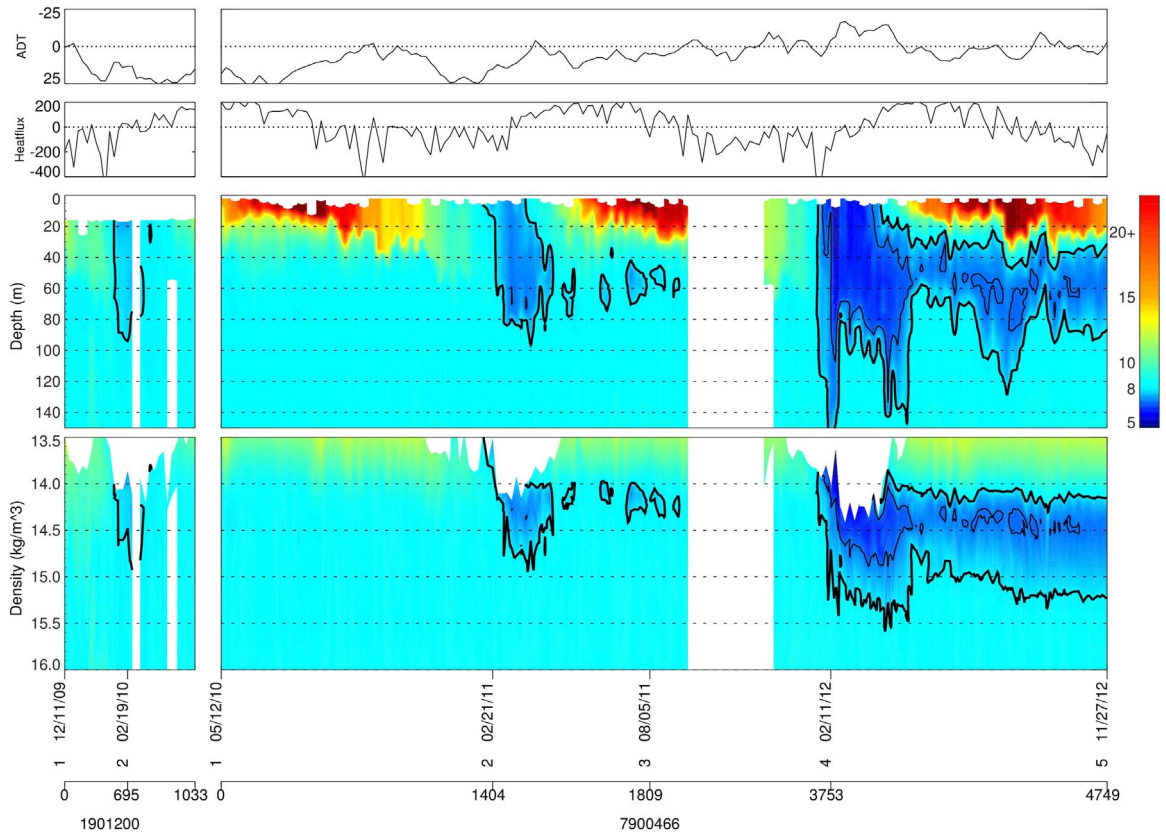

Fig. 5. Contour plots of temporal temperature variation vs depth within the upper 150 m plotted above contour plots of temperature variation vs density (kg m^{-3}) constructed using different Argo float trajectories along the southern rim current zone during December to April 2009 (float 1901200) and along the rim current in the western basin, starting in near the northwestern shelf and continuing towards the south-east (float 7900466). Thick black contour lines mark the 8 °C isotherm which encloses the CIL with colder temperatures, thin black line marks the 7 °C isotherm. White vertical stripes indicate missing data. Dates are given along the x-axis in the form of month/day/year, and the numbers located below the dates refer to float locations as shown in Fig. 3. Float numbers are indicated along the x-axis. The second x-axis represents the distance traveled in km. Above the contour plot absolute dynamic topography (cm) and total heat flux (W/m^2) data along the float trajectory is displayed.

during the following years with some differences. For example, as captured by the float BS0631, the upper 50 m layer of the south-central basin was cooled gradually during the autumn 2003 preconditioning phase, and the old CIL was then replenished with water temperatures of 6.5–7.0 °C in February – early March 2004 (Fig. 2a). The CIL layer covered the upper 80 m layer during the winter formation episode but its lower boundary extended later to 120 m in summer when the float moved towards the Batumi gyre region of the southeastern Black Sea (see Korotaev et al. (2003) for more details on the Batumi gyre structure). Float BS0634 recorded a very similar sequence of events along the southwestern coastal waters (Fig. 2a).

Combining two sets of floats also documented similar events during 2005–2009 within the western-central deep basin (Fig. 2b) and the southeastern deep basin (Fig. 2c). Convection in the cold winter 2006 with temperature characteristics similar to those of 2003 (Fig. 1) led to temperatures of 6.0–6.5 °C within the upper 50 m layer of the west-central basin (see float locations in Fig. 3b). The shallowing of isohalines (Fig. 4) indicate a cyclonic gyre circulation prevailing within this region (Fig. 2b, Location #4 of BS1325 trajectory on Fig. 3b). In contrast to the cyclonic region, the CIL had slightly higher temperatures of 6.5–7.0 °C during winter 2008 and was almost twice as deep (~80 m) within the Batumi anticyclonic region of the southeastern basin (Fig. 2c) (location 15–18 of float BS2619, Fig. 3c). The anticyclonic character of this region may be inferred by deepening of isohalines (Fig. 4) as suggested by the position of 19.0 isohaline at 100 m with respect to its position at 40 m for the west-central basin.

Three markedly different formation episodes depending on the autumn-winter heat flux intensity are demonstrated in Figs. 2b, and 2c. Following a rather weak cooling phase (less than 200 W m^{-2}) in autumn 2005, the mixed layer deepening was limited to 30 m in January 2006. But the subsequent strong cooling event up to 400 W m^{-2} during February led to an abrupt development of 50 m deep mixed layer with temperatures around 6.0 °C (Fig. 2b). In this case of weak preconditioning, the CIL core appeared to be less affected by vertical mixing with the thermocline waters across its upper surface.

The presence of surface waters well above 8 °C indicates no appreciable CIL replenishment in autumn 2006 – January 2007 (Figs. 2b and 2c). Apparently, the cooling events during autumn 2006 eroded the summer thermocline and formed a homogeneous water mass by mixing thermocline waters with the remnant of older CIL waters. The CIL structure extended to 60 m depth with characteristic temperatures of the previous summer. The absence of an additional strong cooling event during February and early March 2007 hindered further deepening and cooling of this layer. On the other hand, autumn 2007-winter 2008 represented a relatively strong CIL formation episode in response to a strong and long-lasting cooling phase that eroded the subsurface CIL layer structure left from the previous year (Fig. 2c). As a major difference to the previous year, equally strong cooling episodes continued in February and early-March 2008 and promoted further deepening of the winter mixed layer leading to a new and fresh cold water mass structure of ~7 °C temperature and 80 m thickness (Fig. 2c) similarly to the cooling events observed in 2003 (Fig. 2a).

The distribution of cold waters with respect to density suggests that in cyclones CIL intrusion was observed down to 15.5 kg m^{-3} (Fig. 2a and Fig. 2b) whereas in the rim current periphery and anticyclones it was within limits of 14.5–15 kg m^{-3} (Fig. 2c). The lower boundary of the CIL is generally located at ~15.4 kg m^{-3} (Fig. 2a, Fig. 2b and BS1550 on Fig. 2c).

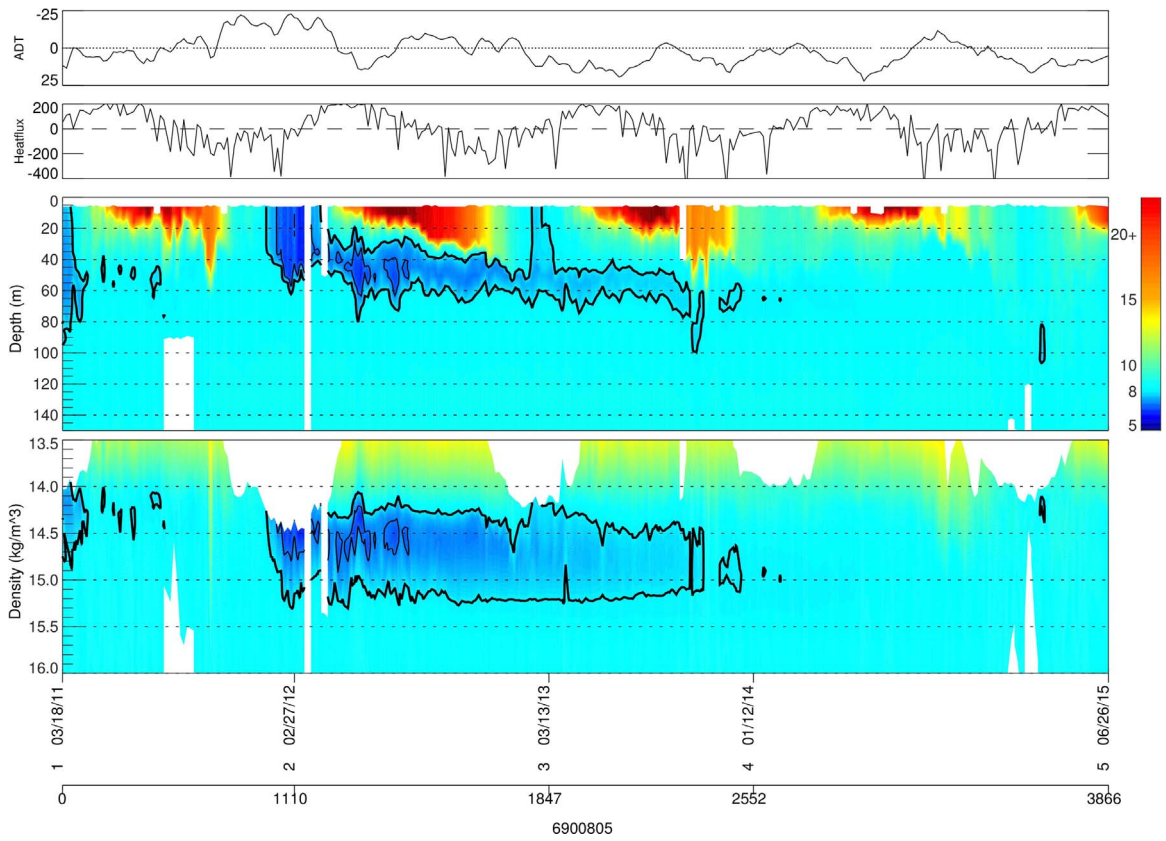

Fig. 6. Contour plot of temporal temperature variation vs depth within the upper 150 m layer plotted above contour plots of temperature variation vs density (kg m^{-3}) using the Argo float 6900805 trajectory along the rim current and central interior basin from March 2011 to June 2015. Thick black contour lines mark the 8 °C isotherm which encloses the CIL with colder temperatures, thin black line marks the 7 °C isotherm. White vertical stripes indicate missing data. Dates are given along the x-axis in the form of month/day/year, and the numbers located below the dates refer to float locations as shown in Fig. 3. Float numbers are indicated along the x-axis. The second x-axis represents the distance traveled in km. Above the contour plot absolute dynamic topography (cm) and total heat flux (W/m^2) data along the float trajectory is displayed.

Winter 2010 encountered a deep CIL replenishment down to 100 m (Fig. 5), even though the event was rather weak. December 2009-January 2010 involved a decent preconditioning phase with mixed layers ~40 m, gradually deepening down to 60 m in January with temperatures just above 8 °C. Due to absence of further cooling events in February and March, layer replenishment was limited to February only, with CIL characteristic temperatures slightly below 8 °C. A stronger CIL replenishment took place in autumn 2010-winter 2011. Even though the preconditioning phase was similar to the one in the previous winter, further cooling during February-March 2011 led to a prolonged replenishment period with temperatures ~7.2 °C. The resulting CIL water mass was centered around 14.5 km m^{-3} and extended to 15.0 km m^{-3}. A thin, non-uniform CIL was observed (Fig. 5 and Fig. 6) in the following months as remnant of this renewal period.

The data from all six active floats during winter 2012 (but only 2 shown here) represented an intense CIL formation episode owing to intense cooling (Fig. 5 and Fig. 6) in very different parts of the Black Sea (Fig. 8). They were subject to a strong and long-lasting preconditioning phase and the subsequent winter cooling in February to form in cold water masses with temperatures less than 7 °C. But those occurring within coastal anticyclones were subject to stronger vertical mixing due to weaker stability of the upper layer water column and able to ventilate the water column down to ~150 m (Fig. 5). The lower boundary of this CIL water mass later resided at 80–100 m. In contrast, the CIL formation that occurred within cyclonic gyres was limited to 60 m (Fig. 6) and preserved this position during the subsequent summer.

Winter 2013 as well as winter 2014 represented another two cases of weak CIL formation episodes with sea surface temperatures slightly colder than 8 °C (Fig. 6 and Fig. 7) inside the western cyclonic gyre (Fig. 8). Out of 5 float measurements of temperature for winter 2013, only two showed enough cooling to renew CIL in the western cyclonic gyre, whereas the other three represented coastal anticyclonic conditions and indicated the absence of CIL formation in warm years in anticyclones or the entire Eastern Black Sea. In winter 2014 10 active floats did not show any significant CIL formation except few chimney-like replenishment events within the upper 40 m along the Western Anatolian Coast by 2 floats. Similarly, no large scale CIL replenishment was observed except some local events in the eastern part of the Black Sea (Fig. 7b), around Sevastopol eddy (Fig. 8b). It should be noted that the lower boundary of the CIL was at ~15.4 kg m^{-3} in previous year's (Fig. 2) while after 2012 it is located ~15.1–15.2 kg m^{-3} (Fig. 6 and Fig. 7), displaying a distinctive trend towards lighter densities.

Out of 12 floats, 6 documented cold water formation during winter 2015, all exclusively in the western part of the Black Sea following a rather long preconditioning phase with sea surface temperatures slightly above 8 °C by the end of January (Fig. 7, Point 4). Five of these showed shallow (~40 m) cold water renewal processes inside the western cyclonic gyre and only one documented the formation event at a coastal site.

4. Conclusions

The Argo profiling floats measurements performed weekly during 2002–2015 provided an unprecedented opportunity for gaining new insights into the formation and annual structure of the cold intermediate water mass in the Black Sea. The period of float measurements corresponded to the climatic warming phase that started in the early 1990s following a previous cooling phase during the 1980s. Strong decadal-scale SST and CIL temperature changes up to 1.5 °C (Oguz

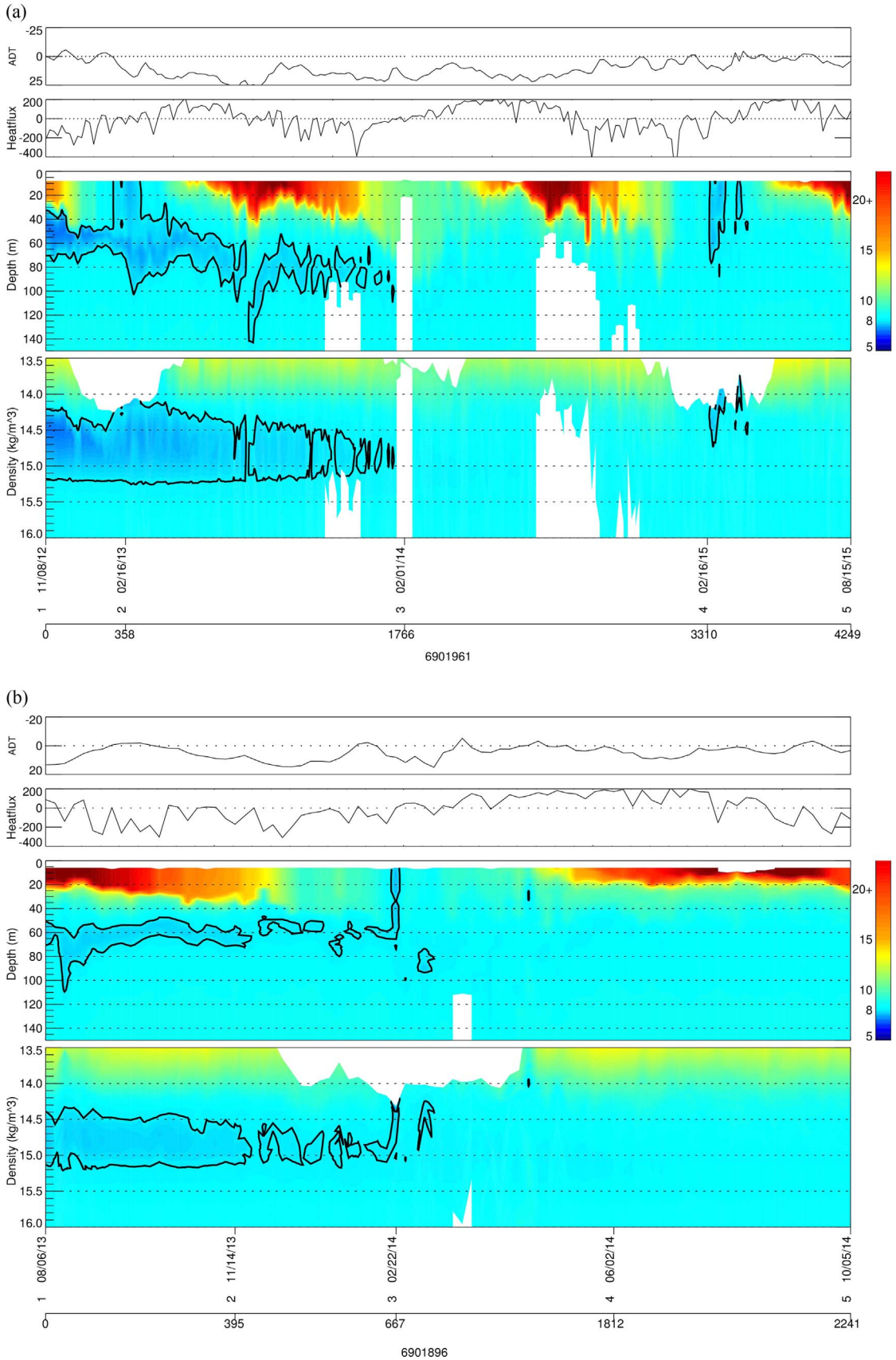

Fig. 7. Contour plots of temporal temperature variation vs depth within the upper 150 m layer plotted above contour plots of temperature variation vs density (kg m^{-3}) constructed using different Argo float trajectories trajectories along the entire rim current during (a) November 2012 to August 2015 (float 6901961) within the west-central basin and (b) continuing to the southeast basin (float 6901896). Thick black contour lines mark the 8 °C isotherm which encloses the CIL with colder temperatures, thin black line marks the 7 °C isotherm. White vertical stripes indicate missing data. Dates are given along the x-axis in the form of month/day/year, and the numbers located below the dates refer to float locations as shown in Fig. 3. Float numbers are indicated along the x-axis. The second x-axis represents the distance traveled in km. Above the contour plot absolute dynamic topography (cm) and total heat flux (W/m^2) data along the float trajectory is displayed.

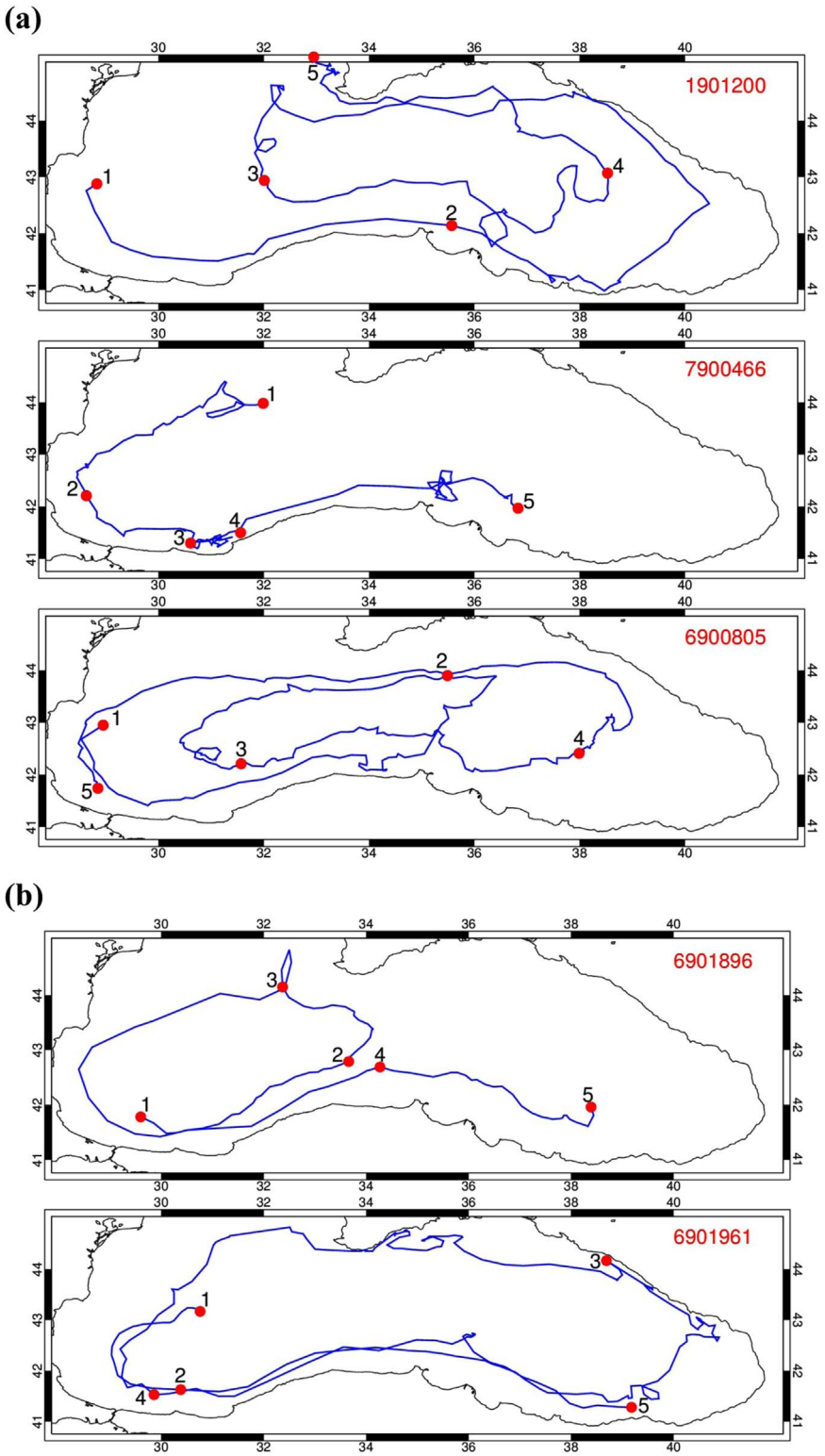

Fig. 8. Argo float trajectories of different floats (a) floats 1901200, 7900466, 690805 used in Fig. 5 and Fig. 6, and (b) 6901896, 6901961 used in Fig. 7. Numbers correspond to the locations of the float marked by dates shown in the temperature transects.

et al., 2006; Oguz, 2011) characterized these successive cooling and warming phases. The float data documented details of interannual variability in the cold water formation episodes depending on the intensity, duration, and frequency of atmospheric cooling events. Particularly strong formation events took place during the winters of 2003, 2006 and 2012 with mean temperatures less than 6.7 °C as compared to the moderate events with mean temperatures in the range of 6.7–7.4 °C during winters of 2004, 2005, 2008, 2011, and weak events with mean temperatures greater than 7.4 °C in 2007, 2010, 2013, 2014 and 2015 (Fig. 9a). The characteristics of formation events also varied greatly depending on their locations in either cyclones or anticyclones (Table 2).

Following the CIL water mass formation, irrespective of its intensity, the mean CIL temperatures started increasing first rapidly during

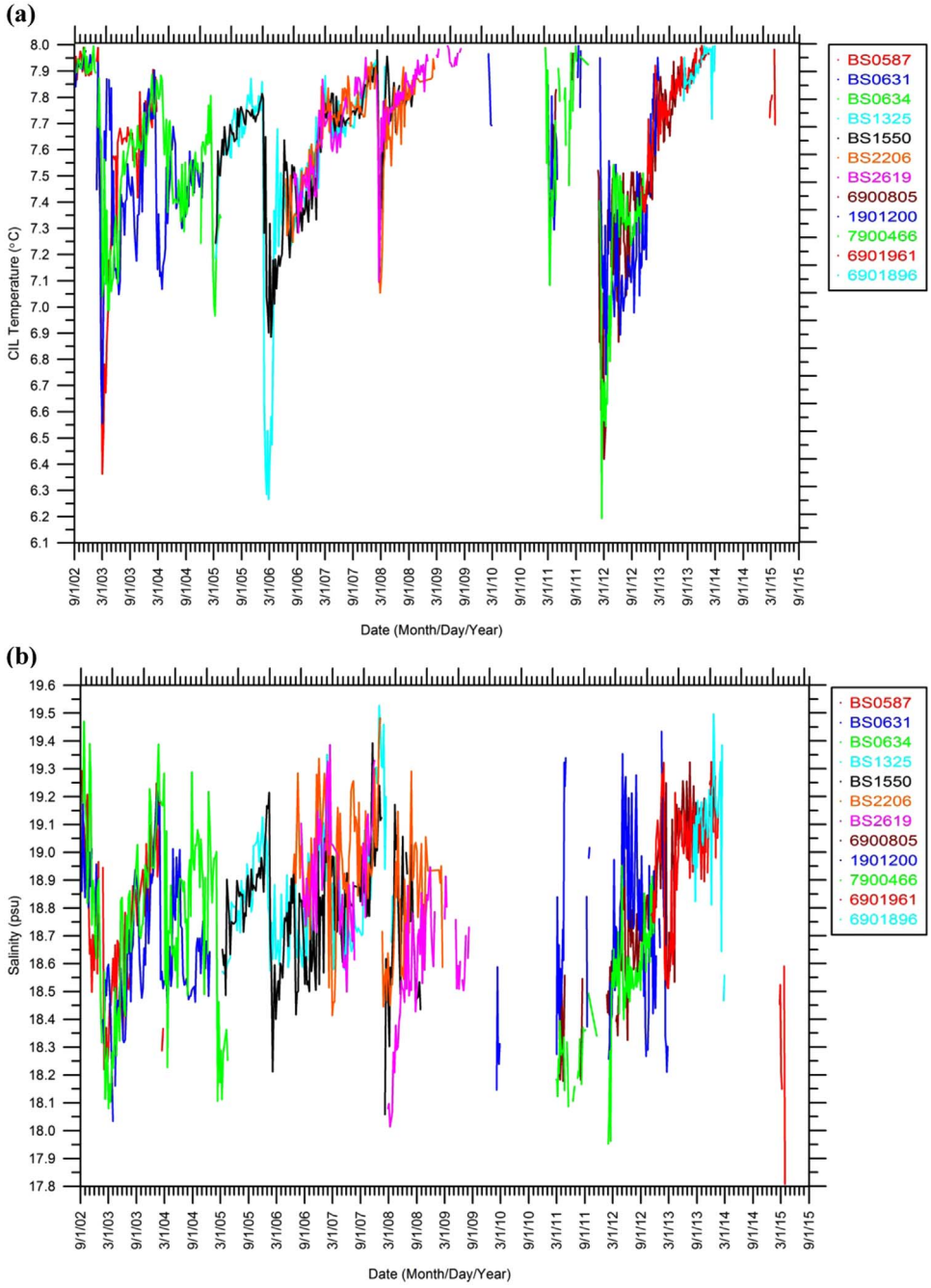

Fig. 9. Temporal variations of (a) the mean CIL temperature representing the average of temperatures measured in each profile that are less than 8 °C and (b) the mean salinity of the CIL for all the available floats during 2002–2015.

March-April and then more gradually to around 7.7–8.0 °C (approaching its 8 °C limit) in the late autumn - early winter prior to a new formation process. This increase in the mean CIL temperature was related to mixing of the cold water mass with those of the thermocline waters above and erosion of the CIL at its lower boundary as well as quasi-lateral mesoscale stirring. Similarly, the average CIL salinity (corresponding to the depth ranges of temperatures less than 8 °C) changed about 1.0 psu during the year. The subsurface salinity values increased gradually from roughly the surface salinity value of 18.0 at the time of formation to about 19.0 towards the end of the year as the CIL turned into the subsurface water mass near the permanent pycnocline in response to turbulent mixing and horizontal stirring processes (Fig. 9b). These features were observed persistently for the entire data set and documented important roles of internal turbulent processes (both isopycnal and diapycnal) as well as lateral intrusions via mesoscale processes on the annual CIL characteristics (Zatsepin et al., 2003; Stanev et al., 2014; Ostrovskii et al., 2016).

The present data set elucidated clearly the dependence of the cold water mass formation on the characteristics of the preconditioning phase and the temporal variability of air-sea heat fluxes. In cyclones, surface buoyancy loss is not strong enough to completely erode the doming structure of isopycnals down to the base of the permanent pycnocline at depths corresponding to 16.5 kg m^{-3} isopycnal surface and to generate a deep convective overturning process. Instead, erosion takes place at best to 15.0–15.5 kg m^{-3} isopycnal surface which implies ventilation of upper layer water mass at most to 80 m depth. Due to weaker stability of anticyclones, however, the ventilation there may extend to about 150 m but this is also limited to isopycnals shallower

Table 2
Characteristics of different cold intermediate water formation events observed in Argo data.

Air-sea heat loss (W/m^2)	State	Type of formation	CIL core temperature	CIL lower boundary	Region of formation	Observed years	Notes
Weak (<100)	Anti-cyclone	No formation	–	–	–	–	–
Weak	Cyclone	Very weak	Just below 8 °C (7.7–7.9)	~40 m	Western Cyclonic Gyre	2007, 2014	No formation in the East
Moderate (100 − 300)	Cyclone	Moderate	7–7.6 °C	40–60 m	Western and Eastern Gyre	2004, 2005, 2008, 2011, 2015	After 2013, CIL core temperatures are slightly below 8 °C.
Moderate	Anti-cyclone	Very weak	Just below 8 °C	60–80 m	Anti-cyclones west of 38°E.	2010, 2011, 2013, 2014, 2015	No formation observed in the eastern Black Sea.
Intense (>300)	Cyclone	Strong	Below 7 °C	60–80 m	Western and Eastern Gyre	2003,2006,2012	–
Intense	Anti-cyclone	Strong	Below 7 °C	>100 m	Anti-cyclones throughout the basin.	2003, 2012	Anticyclones in the east have warmer CIL core temperatures (Above 7 °C)

than 15.5 kg m^{-3}. The demonstration of CIL formation within anticyclonic regions during more intense cold years (e.g. 2003, 2006, 2012) is a new feature which has not been documented in such a great detail previously (Table 2). In either case, the general formation cycle depends on the intensity and duration of the air-sea heat fluxes and local circulation features. Despite its high temporal and spatial variability, the lower boundary of CIL was shifted from its deepest position at the 15.4 kg m^{-3} isopycnal in 2002–2008 to 15.1–15.2 kg m^{-3} isopycnal surfaces after 2012, suggesting an overall freshening in the CIL structure. This finding supports previous work discussing the reduction of ventilation (Pakhomova et al., 2014; Capet et al., 2016).

Earlier modelling studies suggested that mesoscale eddies play an important role in the distribution of CIL as well as contribution to its formation (through heat exchange with the atmosphere), and penetration of the surface cold water into the pycnocline (Stanev and Staneva, 2001; Staneva and Staneva, 2002). Measurements in the northeastern Black Sea (Piotukh et al., 2011) have shown that the heat content of coastal features is almost twice that of offshore waters, emphasizing the relative importance of coastal features.

The convective mixing phase over the domes of interior cyclonic gyres is followed by an isopycnal spreading phase of the newly formed cold water mass toward the periphery of the basin (Oguz and Besiktepe, 1999), where it was distributed by the rim current circulation over the entire basin. Float trajectories in this study pointed to a remarkable persistence of the rim current at interannual time scales, as well as various cyclonic/anticyclonic structures connected by intense jets, and a ubiquitous eddy field (Fig. 3 and Fig. 8). Entrapments of floats within coastal anticyclones at monthly-yearly time scales, however, imply their relatively slow drift around the basin via the rim current whereas their onshore/offshore excursions by mesoscale features suggest a notable eddy-induced material transport.

The spreading phase is modulated considerably by strong eddying motion involving a series of coastal anticyclonic eddies, rim current meanders and offshore filaments (Korotaev et al., 2003). Following spring warming during which the surface mixed layer was formed, the CIL structure was eroded gradually by vertical mixing between the warm surface waters (> 20 °C) and cold intermediate waters (< 8 °C). This process led to the development of a 15–20 m thick seasonal thermocline. Moreover, the lower boundary of the subsurface CIL structure was typically located at 70–80 m depths within the interior basin as compared to 120–130 m depths towards the peripheral rim current zone and coastal anticyclones (Table 2). Vertical mixing of cold intermediate water mass with those of the seasonal thermocline and permanent pycnocline modified its temperature and salinity properties during the rest of the year following the formation episodes with differences up to 1 °C and 1 psu. Such monthly-seasonal changes in the CIL temperature may introduce some uncertainty in the summer-autumn mean CIL temperature variations (Fig. 1a) that was constructed based on the arbitrarily sampled hydrographic data during May-November.

Acknowledgements

This study was supported in part by DEKOSIM (BAP-08-11-DPT2012K120880) funded by the Turkish Ministry of Development. Deployment of six Argo profiling floats 2002–2006 was realized as a result of the collaboration between the US Office of Naval Research, School of Oceanography – University of Washington, Institute of Marine Sciences – Middle East Technical University, and Marine Hydrophysical Institute – Ukranian Academy of Sciences to support the Black Sea GOOS Program.

References

Alkan, A., Zengin, B., Serdar, S., Oguz, T., 2013. Long-term (2001–2011) temperature, salinity and chlorophyll-a variations at a southeastern coastal site of the Black Sea. Turk. J. Fish. Aquat. Sci. 13 (1), 57–68. http://dx.doi.org/10.4194/1303-2712-v13_1_08.

Argo, 2000. Argo float data and metadata from Global Data Assembly Centre (Argo GDAC). SEANOE. http://dx.doi.org/10.17882/42182.

ARGO Science Team, 2000. Report on the Argo science team In: Proceedings of the Second Meeting (AST-2) March 7–9, 2000, Southampton Oceanography Centre, Southampton, UK.

Belokopytov, V.N., 2011. Interannual variations of the renewal of waters of the cold intermediate layer in the Black Sea for the last decades. Phys. Oceanogr. 20 (5), 347–355. http://dx.doi.org/10.1007/s11110-011-9090-x.

Capet, A., Barth, A., Beckers, J.M., Marilaure, G., 2012. Interannual variability of Black Sea's hydrodynamics and connection to atmospheric patterns. Deep Sea Res. Part II: Top. Stud. Oceanogr. 77, 128–142. http://dx.doi.org/10.1016/j.dsr2.2012.04.010.

Capet, A., Troupin, C., Carstensen, J., Grégoire, M., Beckers, J.M., 2014. Untangling spatial and temporal trends in the variability of the Black Sea cold intermediate layer and mixed layer depth using the DIVA detrending procedure. Ocean Dyn. 64 (3), 315–324. http://dx.doi.org/10.1007/s10236-013-0683-4.

Capet, A., E. Stanev, E., Beckers, J.M., Murray, J.W., Grégoire, M., 2016. Decline of the Black Sea oxygen inventory. Biogeosciences 13, 1287–1297. http://dx.doi.org/10.5194/bg-13-1287-2016.

Gregg, M.C., Yakushev, E., 2005. Surface ventilation of the Black Sea's cold intermediate layer in the middle of the western gyre. Geophys. Res. Lett. 32 (3), L03604. http://dx.doi.org/10.1029/2004GL021580.

Kazmin, A.S., Zatsepin, A.G., Kontoyiannis, H., 2010. Comparative analysis of the long-term variability of winter surface temperature in the Black and Aegean Seas during 1982–2004 associated with the large-scale atmospheric forcing. Int. J. Climatol. 30 (9), 1349–1359. http://dx.doi.org/10.1002/joc.1985.

Korotaev, G., Oguz, T., Riser, S., 2006. Intermediate and deep currents of the Black Sea obtained from autonomous profiling floats. Deep Sea Res. Part II: Top. Stud. Oceanogr. 53 (17), 1901–1910. http://dx.doi.org/10.1016/j.dsr2.2006.04.017.

Korotaev, G.K., Knysh, V.V., Kubryakov, V.V., 2014. Study of formation process of cold intermediate layer based on reanalysis of Black Sea hydrophysical fields for 1971–1993. Izv. Atmos. Ocean. Phys. 50 (1), 35–48. http://dx.doi.org/10.1134/S0001433813060108.

Korotaev, G.K., Oguz, T., Nikiforov, A., Koblinsky, C.J., 2003. Seasonal, interannual and mesoscale variability of the Black Sea upper layer circulation derived from altimeter data. J. Geophys. Res. 108, 3122. http://dx.doi.org/1029/2002JC001508).

Krivosheya, V.G., Moskalenko, L.V., Melnikov, V.A., Skirta, A.Y., 2012. Effects of the wind and thermal conditions variability on the structure and dynamics of the seawater in the Northeastern Black Sea. Oceanology 52 (4), 453–466. http://dx.doi.org/10.1134/S0001437012030071.

Kutiel, H., Benaroch, Y., 2002. North Sea-Caspian Pattern (NCP) – an upper level atmospheric teleconnection affecting the Eastern Mediterranean: identification and definition. Theor. Appl. Climatol. 71 (1–2), 17–28. http://dx.doi.org/10.1007/s704-002-8205-x.

MEDOC Group, 1970. Observation of formation of deep water in the Mediterranean Sea, 1969. Nature 227, 1037–1040. http://dx.doi.org/10.1038/2271037a0.

Mihailov, M.E., Stefan, S., Diaconu, V., Lazar, L., 2016. Longterm variability of the water mass structure on the Romanian black Sea shelf. Rom. Rep. Phys. 68 (1), 377–392.

Murray, J.W., Top, Z., Özsoy, Z., 1991. Hydrographic properties and ventilation of the Black Sea. Deep Sea Res. Part A Oceanogr. Res. Pap. 38, S663–S689. http://dx.doi.org/10.1016/S0198-0149(10)80003-2.

Oguz, T., 2002. Role of physical processes controlling oxycline and suboxic layer structures in the Black Sea. Glob. Biogeochem. Cycles 16 (2). http://dx.doi.org/10.1029/2001GB001465.

Oguz, T., 2011. Impacts of climate change on the Black Sea. In: Climate Change and Marine Ecosystem Research: Synthesis of European Research on the Effects of Climate Change on Marine Environments. Marine Board Special Report, pp. 120–127.

Oguz, T., Besiktepe, S., 1999. Observations on the Rim Current structure, CIW formation and transport in the western Black Sea. Deep Sea Res. Part I: Oceanogr. Res. Pap. 46 (10), 1733–1753. http://dx.doi.org/10.1016/S0967-0637(99)00028-X.

Oguz, T., Dippner, J.W., Kaymaz, Z., 2006. Climatic regulation of the Black Sea hydro-meteorological and ecological properties at interannual-to-decadal time scales. J. Mar. Syst. 60 (3), 235–254. http://dx.doi.org/10.1016/j.jmarsys.2005.11.011.

Oguz, T., Latun, V.S., Latif, M.A., Vladimirov, V.V., Sur, H.I., Markov, A.A., Ozsoy, E., Kotovshchikov, B.B., Eremeev, V.V., Unluata, U., 1993. Circulation in the surface and intermediate layers of the Black Sea. Deep Sea Res. Part I: Oceanogr. Res. Pap. 40 (8), 1597–1612. http://dx.doi.org/10.1016/0967-0637(93)90018-X.

Oguz, T., Aubrey, D.G., Latun, V.S., Demirov, E., Koveshnikov, L., Diaconu, V., Sur, H.I., Besiktepe, S., Duman, M., Limeburner, R., Eremeev, V., 1994. Mesoscale circulation and thermohaline structure of the Black Sea observed during HydroBlack'91. Deep Sea Res. Part I: Oceanogr. Res. Pap. 41 (4), 603–628. http://dx.doi.org/10.1016/0967-0637(94)90045-0.

Ostrovskii, A.G., Zatsepin, A.G., 2016. Intense ventilation of the Black Sea pycnocline due to vertical turbulent exchange in the Rim Current area. Deep-Sea Res. I 116, 1–13. http://dx.doi.org/10.1016/j.dsr.2016.07.011.

Ovchinnikov, I.M., Popov, Yu.I., 1987. Evolution of the cold intermediate layer in the Black Sea. Oceanology 27 (1987), 555–560.

Ozsoy, E., Unluata, U., 1997. Oceanography of the Black Sea: a review of some recent results. Earth Sci. Rev. 42 (4), 231–272. http://dx.doi.org/10.1016/S0012-8252(97)81859-4.

Pakhomova, S., Vinogradova, E., Yakushev, E., Zatsepin, A., Shtereva, G., Chasovnikov, V., Podymov, O., 2014. Interannual variability of the Black Sea Proper oxygen and nutrients regime: the role of climatic and anthropogenic forcing. Estuar. Coast. Shelf Sci. 140, 134–145. http://dx.doi.org/10.1016/j.ecss.2013.10.006.

Piotukh, V.B., Zatsepin, A.G., Kazmin, A.S., Yakubenko, V.G., 2011. Impact of the Winter Cooling on the Variability of the Thermohaline Characteristics of the Active Layer in the Black Sea. Oceanology 51 (2), 221–230. http://dx.doi.org/10.1134/S0001437011020123.

Polonsky, A.B., Bardin, M., Yu, Voskresenskaya, E.N., 2007. Statistical characteristics of cyclones and anticyclones over the Black Sea in the second half of the 20th century. Phys. Oceanogr. 17 (6), 348–359. http://dx.doi.org/10.1007/s11110-008-9002-x.

Rayner, N.A., Parker, D.E., Horton, E.B., Folland, C.K., Alexander, L.V., Rowell, D.P., Kent, E.C., Kaplan, A., 2003. Global analyses of sea surface temperature, sea ice, and night marine air temperature since the late nineteenth century. J. Geophys. Res. 108 (D14), 4407. http://dx.doi.org/10.1029/2002JD002670.

Smith, R.O., Bryden, H.L., Stansfield, K., 2008. Observations of new western Mediterranean deep water formation using Argo floats 2004–2006. Ocean Sci. 4 (2), 133–149. http://dx.doi.org/10.5194/os-4-133-2008.

Stanev, E.V., Staneva, J.V., 2001. The sensitivity of the heat exchange at sea surface to meso and sub-basin scale eddies: model study for the Black Sea. Dyn. Atmos. Oceans 33, 163–189. http://dx.doi.org/10.1016/S0377-0265(00)00063-4.

Stanev, E.V., Bowman, M.J., Peneva, E.L., Staneva, J.V., 2003. Control of Black Sea intermediate water mass formation by dynamics and topography: comparison of numerical simulations, surveys and satellite data. J. Mar. Res. 61, 59–99. http://dx.doi.org/10.1357/002224003321586417.

Stanev, E.V., He, Y., Grayek, S., Boetius, A., 2013. Oxygen dynamics in the Black Sea as seen by Argo profiling floats. Geophys. Res. Lett. 40 (12), 3085–3090. http://dx.doi.org/10.1002/grl.50606.

Stanev, E.V., He, Y., Staneva, J., Yakushev, E., 2014. Mixing in the Black Sea detected from the temporal and spatial variability of oxygen and sulfide – Argo float observations and numerical modelling. Biogeosciences 11, 5707–5732. http://dx.doi.org/10.5194/bg-11- 5707-2014.

Staneva, E.V., Staneva, J.V., 2002. Water mass formation in the Black Sea during 1991–1995. J. Mar. Syst. 32, 199–218. http://dx.doi.org/10.1016/S0924-7963(02)00038-6.

The LIWEX Group, 2003. The levantine intermediate water experiment (LIWEX) group: levantine basin—a laboratory for multiple water mass formation processes. J. Geophys. Res. 108, 8101. http://dx.doi.org/10.1029/2002JC001643, C9.

Valchev, N.N., Trifonova, E.V., Andreeva, N.K., 2012. Past and recent trends in the western Black Sea storminess. Nat. Hazards Earth Syst. Sci. 12, 961–977. http://dx.doi.org/10.5194/nhess-12-961-2012.

Zatsepin, A.G., Ginzburg, A.I., Kostianoy, A.G., Kremenetskiy, V.V., Krivosheya, V.G., Stanichny, S.V., Poulain, P.M., 2003. Observations of Black Sea mesoscale eddies and associated horizontal mixing. J. Geophys. Res. (Oceans) 108 (C8), 1978–2012. http://dx.doi.org/10.1029/2002JC001390.

Zatsepin, A.G., Golenko, N.N., Korzh, A.O., Kremenetskii, V.V., Paka, V.T., Poyarkov, S.G., Stunzha, P.A., 2007. Influence of the dynamics of currents on the hydrophysical structure of the waters and the vertical exchange in the active layer of the Black Sea. Oceanology 47, 301–312. http://dx.doi.org/10.1134/S0001437007030022.